Redox Biology 54 (2022) 102356

Contents lists available at ScienceDirect

Redox Biology

journal homepage: www.elsevier.com/locate/redox

# *BRCA1* haploinsufficiency promotes chromosomal amplification under Fenton reaction-based carcinogenesis through ferroptosis-resistance

Yingyi Kong [a], Shinya Akatsuka [a], Yashiro Motooka [a], Hao Zheng [a], Zhen Cheng [a], Yukihiro Shiraki [b], Tomoji Mashimo [c,d], Tatsuhiko Imaoka [e], Shinya Toyokuni [a,f,*]

[a] Department of Pathology and Biological Responses, Nagoya University Graduate School of Medicine, 65 Tsurumai-cho, Showa-ku, Nagoya, 466-8550, Japan
[b] Department of Tumor Pathology, Nagoya University Graduate School of Medicine, 65 Tsurumai-cho, Showa-ku, Nagoya, 466-8550, Japan
[c] Division of Animal Genetics, Laboratory Animal Research Center, Institute of Medical Science, The University of Tokyo, Tokyo, 108-8639, Japan
[d] Division of Genome Engineering, Center for Experimental Medicine and Systems Biology, Institute of Medical Science, The University of Tokyo, Tokyo, 108-8639, Japan
[e] Department of Radiation Effects Research, National Institute of Radiological Sciences, National Institutes for Quantum Science and Technology, 4-9-1, Anagawa, Inage-ku, Chiba, 263-8555, Japan
[f] Center for Low-temperature Plasma Sciences, Nagoya University, Furo-cho, Chikusa-ku, Nagoya, 464-8603, Japan

ARTICLE INFO

*Keywords:*
BRCA1
Iron
Renal cell carcinoma
Chromosomal amplification
Mitochondria

ABSTRACT

Germline-mutation in *BRCA1* tumor suppressor gene is an established risk for carcinogenesis not only in females but also in males. Deficiency in the repair of DNA double-strand breaks is hypothesized as a responsible mechanism for carcinogenesis. However, supporting data is insufficient both in the mutation spectra of cancers in the patients with *BRCA1* germline-mutation and in murine knockout/knock-in models of *Brca1* haploinsufficiency. Furthermore, information on the driving force toward carcinogenesis in *BRCA1* mutation carriers is lacking. Here we applied Fenton reaction-based renal carcinogenesis to a rat heterozygously knockout model of *BRCA1* haploinsufficiency (mutant [MUT] model; *L63X/+*). Rat MUT model revealed significant promotion of renal cell carcinoma (RCC) induced by ferric nitrilotriacetate (Fe-NTA). Array-based comparative genome hybridization of the RCCs identified significant increase in chromosomal amplification, syntenic to those in breast cancers of *BRCA1* mutation carriers, including *c-Myc*, in comparison to those in the *wild-type*. Subacute-phase analysis of the kidney after repeated Fe-NTA treatment in the MUT model revealed dysregulated iron metabolism with mitochondrial malfunction assessed by expression microarray and electron microscopy, leading to renal tubular proliferation with iron overload. In conclusion, we for the first time demonstrate that biallelic *wild-type BRCA1* provides more robust protection for mitochondrial metabolism under iron-catalyzed oxidative stress, preventing the emergence of neoplastic cells with chromosomal amplification. Our results suggest that oxidative stress via excess iron is a major driving force for carcinogenesis in BRCA1 haploinsufficiency, which can be a target for cancer prevention and therapeutics.

## 1. Introduction

Historically, tumor suppressor genes were identified one by one through the genetic analysis of cancer-prone kins [1]. *BRCA1*, cloned in 1994 as one of them [2], imposes a high risk, if one of the germline alleles is inactivated, not only for breast/ovarian carcinoma in females but also for breast, prostate [3] and probably pancreatic/stomach cancer in males [4]. Currently, this risk is clinically well recognized [5], and guidelines recommend risk-reducing bilateral mastectomy and salpingo-oophorectomy in the early life of women [6], which requires further consideration of novel strategies for higher quality of life. Furthermore, a viewpoint has been lacking on what is the causative or promoting agents for the carcinogenesis of *BRCA1* mutation carriers, considering that not all the mutation carriers obtain carcinoma(s).

Many mouse *Brca1* haploinsufficiency models have been generated since the 1990's. However, expected phenotypes were not obtained presumably due to the species difference and the short lifetime period [7]. Our laboratory is aware that even the difference of *Mus musclus* (mouse) and *Rattus norvegicus* (rat) within rodents provides us with a different tendency in the same carcinogenesis model, suggesting more proximity of rats to humans in phenotype than mice [8]. Recently, a rat

* Corresponding author. Department of Pathology and Biological Responses, Nagoya University Graduate School of Medicine, 65 Tsurumai-cho, Showa-ku, Nagoya, Japan.
*E-mail address:* toyokuni@med.nagoya-u.ac.jp (S. Toyokuni).

https://doi.org/10.1016/j.redox.2022.102356
Received 11 May 2022; Accepted 25 May 2022
Available online 28 May 2022

**Abbreviations**

| | |
|---|---|
| aCGH | array-based comparative genome hybridization |
| BAP1 | BRCA1-assciated protein 1 |
| *BRCA1* MUT | *BRCA1* heterozygously knockout, indicating *Brca1 (L63X/+)*, in this work |
| CT | computed tomography |
| Fe-NTA | ferric nitrilotriacetate |
| FFPE | formalin-fixed paraffin-embedded |
| FISH | fluorescent *in situ* hybridization |
| GPX4 | glutathione peroxidase 4 |
| HNE | 4-hydroxy-2-nonenal |
| ip | intraperitoneal(ly) |
| Mcub | mitochondrial calcium uniporter dominant negative subunit β |
| MRI | magnetic resonance imaging |
| MUT | mutant |
| ns | not significant (statistically) |
| 8-OHdG | 8-hydroxy-2'-deoxyguanosine |
| PBS | phosphate-buffered saline |
| PVDF | polyvinylidene fluoride |
| RCC | renal cell carcinoma |
| RIPA | radioimmunoprecipitation assay |
| RT | room temperature |
| SDS-PAGE | sodium dodecyl sulfate polyacrylamide gel electrophoresis |
| SSC | saline sodium citrate |
| TfR1 | transferrin receptor 1 |
| WT | *wild-type* |

heterozygous knockout model of *BRCA1* haploinsufficiency (mutant [MUT] model; *L63X/+*) has been established, which revealed a significant enhancement of radiation-induced mammary carcinogenesis in females (*T Imaoka, unpublished data*).

Excess iron is a risk for carcinogenesis [9–13]. The association of breast cancer and excess iron has been previously suggested [11] but is still controversial [14] with deficiency of data. We thus far demonstrated that Fenton reaction-based repeated oxidative stress via ferric nitrilotriacetate (Fe-NTA) in rats [15–18] causes renal cell carcinoma (RCC) [19,20] with genetic alterations similar to those in humans [13,21–24]. In the present study, we applied Fe-NTA-induced rat renal carcinogenesis to the rat *Brca1* MUT model to evaluate the involvement of BRCA1 haploinsufficiency in Fenton reaction-based carcinogenesis from the viewpoint of iron metabolism and the induced genetic alterations at the chromosomal level. We found that *Brca1* haploinsufficiency causes significantly higher mitochondrial dysfunction with iron accumulation after continuous oxidative stress, which was associated with promoted carcinogenesis and allowed significantly increased chromosomal amplifications, syntenic to those in breast cancers of *BRCA1* mutation carriers [25,26].

## 2. Materials and methods

### 2.1. Materials

$Fe(NO_3)_3 \cdot 12H_2O$ was from Wako (Osaka, Japan) and nitrilotriacetic acid disodium salt was from Tokyo Chemical Industry (Tokyo, Japan). All the chemicals used were of analytical grade.

### 2.2. Rat BRCA1 haploinsufficiency model

A rat heterozygous knockout (mutant; MUT) model of *Brca1* with haploinsufficiency (*L63X/+*; *Jcl:SD*, CLEA Japan, Tokyo) was recently established by the use of CRISPR-Cas9 system (*T Imaoka, unpublished data and will be published separately*), maintained by mating with *wild-type Jcl:SD* rats as heterozygotes, and used in the present study. Rats with homozygously *MUT* alleles *(L63X/L63X)* were embryonic lethal as described in the mouse models [7]. Genotyping was performed with PCR using the following primers: rBrca1-3F, 5'-TGCAGGTAAGTGTAATTTTCATAGG-3'; rBrca1-3R, 5'-CCGATGTGCATGGTACTGTC-3'; rBrca1-TAG-1F, 5'-GGACCTTCCCAGTGTCCTTA-3', where 3F/3R amplified 572 bp *wild-type* allele and TAG-1F/3R amplified 252 bp *MUT* allele. Regarding *Brca1* expression with qPCR analysis, a pair of primers: Brca1-exon3-F, 5'-GGACCTTCCCAGTGTCCTTT-3' and Brca1-exon4-R, 5'-AGCATCAATGATTTTCAGCAGCT-3' (product size 108 bp) were used with a pair of primers for β-Actin: F-5'-ATGAAGTGTGACGTTGACATCCGT-3' and R-5'-CTGCTGGAAGGTGGACAGTGAG-3' (product size: 216 bp).

### 2.3. Renal carcinogenesis experiments with Fe-NTA

$Fe(NO_3)_3 \cdot 12H_2O$ and nitrilotriacetic acid disodium salt were dissolved in deionized water to make 300 mM and 600 mM solutions, respectively, which were mixed immediately before use to make Fe-NTA solution with a ratio of 1:2 (*v/v*), when the pH was adjusted to 7.4 with sodium carbonate [15]. Forty male *wild-type Sprague-Dawley* rats (CLEA Japan; n = 20 for untreated control and n = 20 for carcinogenesis protocol) and 40 male *Brca1(L63X/+)* haploinsufficient rats (MUT; n = 21 for untreated control and n = 19 for carcinogenesis protocol) of the same strain at 4–5 weeks of age were maintained under a standard diet (CE-2; CLEA Japan) at the laboratory animal facility of Nagoya University Graduate School of Medicine. As the renal carcinogenesis protocol, male rats were injected *ip* with Fe-NTA with a dose of 5 mg iron/kg for the first 3 days followed by 7 mg iron/kg for the next 2 days for the first week, 7 mg iron/kg for the first day followed by 5 mg iron/kg for the next 4 days for the second week, 7 mg iron/kg for the first 3 days followed by 10 mg iron/kg for the next 2 days for the third week, and injected with a dose of 10 mg iron/kg 3 times a week during the next 8 weeks (a total of 11 weeks). However, in case the weight of the rat decreased >5% in comparison to the previous injection, the next injection was withheld. The rats which were found to have fatal RCC by palpation or to be dying were euthanized. Computed tomography (CT; SKYSCAN1176, Bruker, Billerica, MA) and magnetic resonance imaging (MRI; MRS 3017 Benchtop MRI Systems; MR Solutions Ltd., Guildford, UK) were used, if necessary, to confirm the presence of RCC. Fresh kidney/RCC tissues were either fixed in 10% phosphate-buffered formalin for hematoxylin & eosin staining/immunohistochemistry/-fluorescent *in situ* hybridization or frozen at −80 °C for the other analyses. Animal experimental committee of Nagoya University Graduate School of Medicine approved all the animal experiments described.

### 2.4. Subacute study

Twenty two male *wild-type Sprague-Dawley* rat (CLEA Japan; n = 5 for untreated control and n = 8 and 9 for carcinogenesis protocol at 1 and 3 week[s], respectively) and 23 male *Brca1(L63X/+)* rat (MUT; n = 5 for untreated control and n = 9 for carcinogenesis protocol at 1 and 3 week [s], respectively) of the same strain at 4 weeks of age were injected *ip* with Fe-NTA with a dose of 5 mg iron/kg for the first two days followed by 7 mg iron/kg for the next three days for the first week, and 10 mg iron/kg 5 times a week for the next 2 weeks. The rats were euthanized 48 h after the final injection. The fresh kidney tissues were excised and processed as described in section 2.3.

### 2.5. Microscopical and electron-microscopical analyses

Tumorous and non-tumorous tissue samples were fixed in phosphate-buffered 10% formalin and embedded in paraffin (FFPE) for the subsequent pathological analyses. For the electron-microscopic analysis, renal cortical area was excised as cubes with 1-mm edge and fixed in 2 mM glutaraldehyde, containing 1 mM phosphate-buffered saline (PBS). Transmission electron microscopy was performed with a JEM-1400PLUS (JEOL; Tokyo, Japan) as described [27,28].

### 2.6. Immunohistochemistry

Immunostainings were performed by BOND MAX/III (Leica, Wetzlar, Germany) with BOND Polymer Refine Detection (ds9800; Leica) as described [29]. Quantitation of immunohistochemical analysis, including Ki67 as a cell proliferation marker [30], was performed as described [31]. Antibodies used are summarized in Table S1.

### 2.7. Array-based comparative genomic hybridization (aCGH)

Genomic DNA from RCC samples was extracted using DNeasy Blood and Tissue Kit (Qiagen GmbH, Hilden, Germany), which was evaluated by NanoDrop2000 (Thermo Fisher Scientific, Waltham, MA). Concentration of dsDNA was quantified with Quant-iT dsDNA BR Assay Kit (Thermo Fisher Scientific). We labeled DNA from 16 rat primary RCCs (4 in *wild-type* without metastasis, 4 in *wild-type* with pulmonary metastasis, 4 in *Brca1-MUT* rat without metastasis, and 4 in *Brca1-MUT* rat with pulmonary metastasis; randomly selected from RCC samples of appropriate size [diameter >15 mm] without massive necrosis and obtained by scheduled autopsy; Table S2) with Cy-5 and the corresponding control DNA with Cy-3, which were applied to the aCGH microarray slides (SurePrint G3 Rat CGH 4 × 180k Microarray, G4826A#27064, Agilent Technologies, Santa Clara, CA) according to the Agilent Oligonucleotide Array-Based CGH for Genomic DNA Analysis protocol Ver.7.3. The image data from Agilent scanner was analyzed with Agilent Feature Extraction Software 10.7.

### 2.8. Fluorescent in situ hybridization (FISH)

FISH was performed on 4 μm-thick FFPE tissue sections using *c-Myc* (Cy3)/Ch7CEN (Spectrum Green) dual color FISH probe (Chromosome Science Laboratory, Sapporo, Japan) as described [32] with modification. Ten additional RCC cases other than those used for aCGH analysis were randomly selected for *wild-type* (n = 5) and *MUT* (n = 5; Tables S2 and S3). Briefly, the slides are pretreated by boiling in 10 mM citric acid buffer (pH 6.0) with microwave for 15 min, followed by treatment with 0.5% pepsin in 0.2 N HCl at 37 °C for 30 min and washing with PBS. The slides were co-denatured with the FISH probe at 80 °C for 10 min and hybridized at 37 °C for 48 h. The slides were washed in 0.4 x saline sodium citrate (SSC)/0.3% Nonidet P-40 at 73 °C for 3 min, followed by 3 times wash with 1 x SSC at room temperature (RT). The slides were thereafter counterstained with Hoechst33342 (Thermo Fisher Scientific) and coverslips were mounted using Vectashield plus (Vector laboratories, Burlingame, CA). The samples were observed with BZ-X800 (Keyence, Osaka, Japan). The amplification was defined as *c-Myc*/Ch7CEN ratio of ≥2 at least in 20 nuclei per RCC cells. The average of *c-Myc*/Ch7CEN ratio was calculated in ≥20 cells per sample.

### 2.9. Expressional microarray analysis

Total RNA was isolated using a RNeasy Mini kit (Qiagen). A total of 16 microarrays (SurePrint G3 Rat Gene Expression v2 8 × 60K Microarray, G4858A#74036, Agilent Technologies; n = 2 for untreated control and n = 3 for carcinogenesis protocol at 1 and 3 week[s] in the male *wild-type Sprague-Dawley* rat and male *Brca1*-MUT rat, respectively) were used. The image data from Agilent scanner was analyzed with Agilent Feature Extraction Software 10.7. The values of signal intensities were normalized by Agilent GeneSpring GX software 13.1. GO term analysis was performed for some subsets of the genes that are differentially expressed between *wild-type* and *Brca1-MUT* groups.

### 2.10. Immunoblot analysis

Tissue or cell pellet was homogenized in RIPA buffer with protease inhibitor as described [33]. The lysates were centrifuged at 15,000 rpm for 15 min at 4 °C. The supernatant was collected and stored at −80 °C. Protein Assay Bicinchoninate kit (Nacalai Tesuqe, Kyoto, Japan) was used to quantify the protein. According to the standard protocol, proteins were separated with SDS-PAGE and transferred onto PVDF membranes, which were incubated in blocking buffer (5% defatted milk) at 4 °C overnight. They were then incubated with the primary antibody for 2 h and then HRP-conjugated secondary antibody for 30 min at RT, followed by reaction with Chemi-Lumi One Ultra or Super kit (Nacalai Tesque). Finally, the bands were visualized with LuminoGraph I (ATTO, Tokyo, Japan) and quantified with ImageJ software (https://imagej.nih.gov/ij/). Antibodies used are summarized in Table S1.

### 2.11. Histological analysis of iron

The evaluation of histological Perl's iron staining for insoluble Fe(III) was performed as described [34]. Regarding analysis of catalytic Fe(II), kidneys of the male *wild-type Sprague-Dawley* rat and male *BRCA1*-MUT rat were excised after carcinogenesis protocol as described in section 2.4. The kidney tissues were embedded in plastic cryomold filled immediately after excision with Optimal Cutting-Temperature compound (Sakura Finetek Japan, Tokyo), using dry ice in acetone. Frozen sections were cut, using cryostat (Leica, CM1520). Then, the detection was performed by applying RhoNox-4 (also as FerroOrange; Dojindo, Kumamoto, Japan) on the kidney frozen sections as described [35], which were observed with a fluorescence microscope (BZ-9000, Keyence, Osaka, Japan). The intensity of fluorescence was evaluated by ImageJ as described [35].

### 2.12. Citrate synthase activity

Citrate synthase activity assay kit (MAK193, Sigma-Aldrich) was used according to the manufacturer's instructions.

### 2.13. Statistical analysis

We performed all the statistical analyses by the use of GraphPad Prism 9 (GraphPad Prism, San Diego, CA). We calculated significance of difference by unpaired *t*-test, *Wilcoxon rank-sum* test, *Pearson's chi-square* test and *Log-rank* (*Mantel-Cox*) test. Significance was defined either as $*P < 0.05$, $**P < 0.01$, $***P < 0.001$ or not significant (ns). Data is shown as means ± SEM unless otherwise specified.

## 3. Results

### 3.1. Brca1 haploinsufficiency significantly promotes Fe-NTA-induced renal carcinogenesis

In the carcinogenesis experiments, no RCC was observed in the untreated control rats both of the *wild-type* (WT) and *Brca1* MUT groups at day 543 after the last injection (day 655 after birth). In contrast, WT and *Brca1* MUT groups under Fe-NTA-induced renal carcinogenesis protocol generated 17/20 (85.0%) and 17/19 (89.5%) of RCCs, respectively (Table 1, Fig. 1A). RCCs of both the WT and *Brca1* MUT groups showed pulmonary metastasis at 47.1% and 35.3%, respectively (Tables 1 and S2), and RCCs of MUT rats showed a higher but statistically not significant incidence of peritoneal invasion/dissemination (35.3% and 52.9%, $P = 0.300$; Tables 1 and S2) with significantly higher Ki-67 cellular

**Table 1**
Summary of Fe-NTA-induced renal carcinogenesis experiments in rats.

| | Untreated control | | Fe-NTA-induced renal carcinogenesis protocol | |
|---|---|---|---|---|
| | *Wild-type* | *Brca1 (L63X/+)* | *Wild-type* | *Brca1 (L63X/+)* |
| Total renal cell carcinoma (RCC) | 0/20 | 0/21 | 17/20 (85.0%) | 17/19 (89.5%) |
| RCC with pulmonary metastasis | 0/0 | 0/0 | 8/17 (47.1%) | 6/17 (35.3%) |
| RCC with peritoneal invasion/dissemination | 0/0 | 0/0 | 6/17 (35.3%) | 9/17 (52.9%) |

Fe-NTA, ferric nitrilotriacetate; *Brca1*(*L63X/+*), *Brca1* mutant (heterozygously knockout) rat. Refer to text for details.

proliferation index (Fig. S1). There was a significant promotional effect of renal carcinogenesis in *Brca1* haploinsufficiency in comparison to WT (Fig. 1A), which was regarded mainly to work at the promotional stage [36] of carcinogenesis (median survival; WT 395 days *vs* MUT 362 days after the last injection; $P < 0.05$). All the tumors we obtained were RCCs (Fig. 1BC), namely adenocarcinoma of renal tubular origin, which are summarized in Table S2 according to the Fuhrman grade of histological classification of human RCCs [37]. Sometimes the RCCs were bilateral and interpreted as independent origin if the histology was different. Of note, all the RCCs from MUT rats revealed BRCA1 expression but with lower phosphorylation (Ser1423, human) with immunoblot analysis, indicating that the remaining *WT* allele is neither deleted nor inactivated during renal carcinogenesis, thus indicating haploinsufficient (Fig. S1). This haploinsufficiency of BRCA1 is quite distinct from other major tumor suppressor genes, such as *Rb, p53* and $p16^{INK4a}$, where the remaining WT allele is inactivated during carcinogenesis [1].

### 3.2. *Brca1 haploinsufficiency significantly increases chromosomal amplifications in Fe-NTA-induced RCCs*

We selected 16 RCCs (4 each from WT RCCs with/without pulmonary metastasis and *Brca1*-MUT RCCs with/without pulmonary metastasis), which were analyzed with aCGH (GEO accession: GSE198508). We observed various genetic alterations at the chromosomal level (Figs. 2A and S2) as we previously reported on the RCCs generated in F1 hybrid rats between *Fischer-344* and *Brown-Norway* strain [23]. In WT RCCs with/without pulmonary metastasis, deletions were significantly prevalent in general but only centromeric portion of chromosome 4 showed significantly frequent amplification, where *c-Met* oncogene was located as we previously described [23] (Figs. 2A and S2).

In contrast, MUT RCCs with/without pulmonary metastasis revealed significantly higher frequency of chromosomal amplification ($P < 0.05$) in comparison to those in WT (Fig. 2A, S2 and S3). Among those, amplification of wide area of chromosome 7 was most prominent in the MUT RCCs (Fig. 2A). Of note, RCCs without pulmonary metastasis revealed more significant difference between WT and MUT ($P < 0.01$; Fig. S3). Whereas WT RCCs revealed homozygous deletion in gene-desert area of chromosome 15, MUT RCCs showed significant amplification (Fig. 2A, blue arrowhead and S2).

### 3.3. *Specific amplification of c-Myc oncogene in the RCCs of Brca1 MUT rats*

Amplification of chromosome 7 in MUT RCCs was syntenic to the locations (human chromosome 8) of breast cancer in *BRCA1* germline-mutated females [26], which led to our identification of *c-Myc* amplification as a major responsible oncogene. We found *c-Myc* amplification in 4 cases (50.0%) of the eight MUT RCCs examined by aCGH. Only one case with pulmonary metastasis (12.5%) out of 8 WT RCCs showed *c-Myc* amplification. Further FISH analysis on *c-Myc* locus confirmed significantly higher incidence of *c-Myc* amplification in the other MUT RCCs in comparison to WT RCCs (4/5 in MUT RCCs *vs* 0/5 in WT RCCs; in total, 8/13 [61.5%] in MUT RCCs *vs* 1/13 [7.7%] in WT RCCs; $P < 0.01$; Table S3) and revealed that *c-Myc* amplification included those in the extrachromosomal DNA (micronuclei) (Fig. 2B, Table S3).

In contrast, frequency of *c-Met* amplification was not statistically different via aCGH analysis between MUT RCCs (2/4 with pulmonary metastasis and 3/4 without metastasis; total 5/8) and WT RCCs (4/4 with pulmonary metastasis and 2/4 without metastasis; total 6/8; $P = 0.590$).

### 3.4. *Brca1 haploinsufficiency causes iron dysregulation in association with mitochondrial malfunction in the subacute phase of Fe-NTA-induced renal carcinogenesis*

To search non-selectively for the possible molecular mechanisms linking BRCA1 haploinsufficiency with the promotion of Fenton reaction-based carcinogenesis and chromosomal amplification, we performed expression microarray analysis at the subacute phase of carcinogenesis at 3 weeks (GEO accession: GSE198507). Differential analysis between WT and MUT at 3 weeks suggested the pathways involved in heme/hemoglobin, oxygen and iron (Fig. 3A, Table S4). Protein levels of Brca1 were significantly increased at 1 week with MUT kidney at a lower level. At 3 weeks, the increased Brca1 protein level showed a significant difference in mRNA (Fig. 3B). Based on the results, we decided to focus on the investigation of mitochondria and iron metabolism. Indeed, various genes revealed significantly altered renal expression between WT and MUT at 3 weeks of Fe-NTA-induced renal carcinogenesis protocol, such as in iron metabolism (*Tf* and *Fth1*), glucose metabolism (*Phkg*), amino acid metabolism (*Got1* and *Lox*), cell cycle inhibition (*Cdkn1a*), hemoglobin (*Hbb, Hba1, Hbe2 and Hbb-b1*) and lipid metabolism (*Aloxe3* and *Acaca*). Expression of mitochondrial calcium uniporter dominant negative subunit beta (*Mcub*) was significantly impaired in MUT (Fig. 3C).

We further performed electron microscopic analysis on mitochondrial morphology, which disclosed that mitochondria are smaller with deformity whereas lysosomal fraction significantly increased even in the untreated MUT kidney. At 3 weeks of the carcinogenesis protocol, mitochondria became significantly sparser, irregular and small-sized with electron-dense deposits and loss of cristae whereas significantly higher lysosomal/autophagosomal fraction was maintained in the *Brca1*-MUT kidney (Fig. 4A–C). This was also confirmed by a decrease in the protein levels regulating mitochondrial fusion (Mitofusion1/2 and Opa1) and fission (Drp1) [38] in the MUT kidney at 3 weeks of the carcinogenesis protocol (Figs. 4 and S4). Paradoxically to the electron microscopic observation, citrate synthase activity as an index of mitochondrial mass was significantly higher in the MUT kidney, suggesting a substantial need for citrate for carcinogenic proliferation. mTOR, a protein associated with mitochondrial biogenesis [39], showed a decrease and p62, an adaptor protein for mitophagy [40], was lower in the MUT kidney at 3 weeks of the carcinogenesis protocol in comparison to the WT kidney (Figs. 4D and S4).

Regarding iron metabolism, we found significantly higher iron deposition in the MUT kidney at 3 weeks of carcinogenesis protocol than WT not only with Perl's iron staining (Fig. 5A) but also with Tf expression (Fig. 5B). This was consistent with a significant increase in Fth1 and a significant decrease in Tfr1 in the MUT kidney at 3 weeks of carcinogenesis protocol in comparison to the WT kidney (Fig. 5C). Significant increase in Tf production in the MUT kidney at 3 weeks of carcinogenesis protocol suggests an establishment of a regulatory system to avoid excess iron.

### 3.5. *Brca1 haploinsufficiency generates carcinogenic environments with ferroptosis-resistance under iron-catalyzed persistent oxidative stress*

Finally, we evaluated the levels of oxidative stress biomarker molecules from the viewpoint of ferroptosis. 8-OHdG [41] was significantly

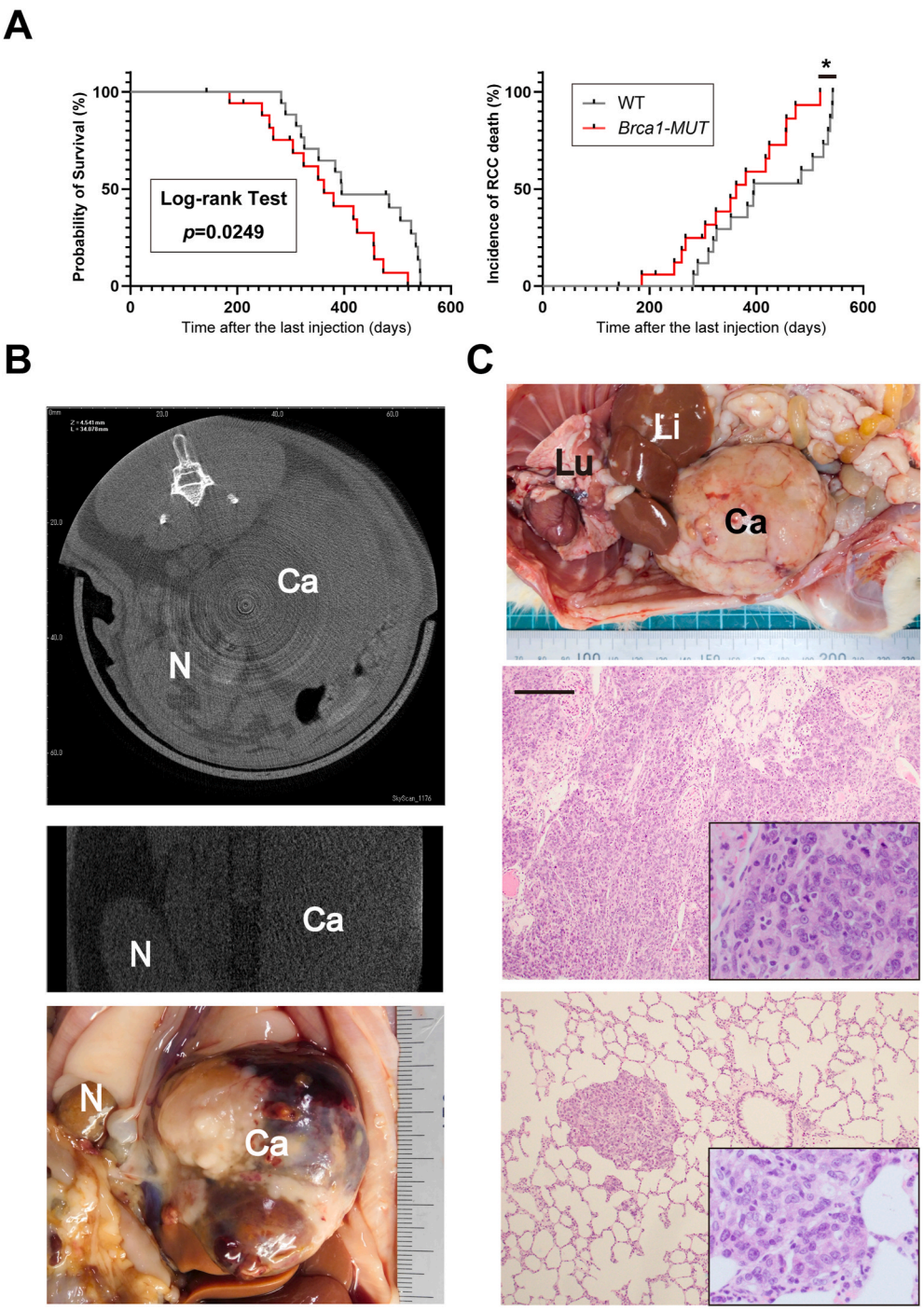


**Fig. 1.** *Brca1* heterozygous knockout (L63X/+) in rat reveals promotional effect under ferric nitrilotriacetate (Fe-NTA)-induced renal carcinogenesis. (A) Probability of survival under Fe-NTA-induced renal carcinogenesis protocol in the *wild-type* (WT; n = 20) and *Brca1* heterozygous knockout$^{L63X/+}$ (Mutant [MUT]; n = 19) groups (MUT *vs* WT; $P < 0.05$). Untreated groups of WT (n = 20) and MUT (n = 21) showed no renal cell carcinoma (RCC) during the experimental period (left panel; refer to Table 1). Probability of RCC-dependent death in the WT and MUT groups under Fe-NTA-induced renal carcinogenesis protocol (right panel; $*P < 0.05$). (B) RCC confirmed by computed tomography (CT) prior to euthanization and autopsy (top panel, transverse section CT; middle panel, coronal section CT; bottom panel, macroscopic appearance of the corresponding RCC). N, normal kidney; Ca, renal cell carcinoma. (C) A case of Fe-NTA-induced RCC in *BRCA1* MUT rat (top panel, macroscopic appearance; middle panel, histology of the primary RCC; bottom panel, histology of pulmonary metastasis of RCC (bar = 200 μm; 50 μm in the inset). Li, liver; Lu, lung.

increased at 3 weeks of carcinogenesis protocol in the MUT kidney with significantly higher Ki-67 cellular proliferation index in comparison to the WT kidney (Fig. 6AB). In contrast, γ-H2AX, a marker for DNA double-strand breaks [42], showed negligible immunostaining in the untreated control kidney of both WT and MUT but significantly increased in the kidney at 3 weeks of carcinogenesis protocol with WT significantly higher than MUT (Fig. 6C), which may be attributed to *Brca1* haploinsufficiency.

HNEJ-1 antibody has been recently established as a tool to detect ferroptosis [29]. Whereas the immunostaining was not different between WT and MUT in the untreated control kidney, WT showed significantly more intense immunostaining than MUT at 3 weeks of carcinogenesis protocol (Fig. 6D), suggesting that MUT kidney is more resistant to ferroptosis under the Fe-NTA-induced renal carcinogenesis protocol. Ferroptosis-resistance at 3 weeks of carcinogenesis protocol in the MUT kidney was confirmed by Cox-2 and ACSL4 (Fig. S5). Catalytic Fe(II) was significantly decreased in the MUT kidney in comparison to the untreated kidney, suggesting an early establishment of ferroptosis-resistance during this period (Fig. S5).

## 4. Discussion

Fe-NTA-induced renal carcinogenesis has been established as an iron-induced carcinogenesis in *wild-type* (WT) rats with similarity of genetic alterations to those in human cancers [13,23,24]. Germline mutation of BRCA1-associated protein 1 (BAP1) is an established risk

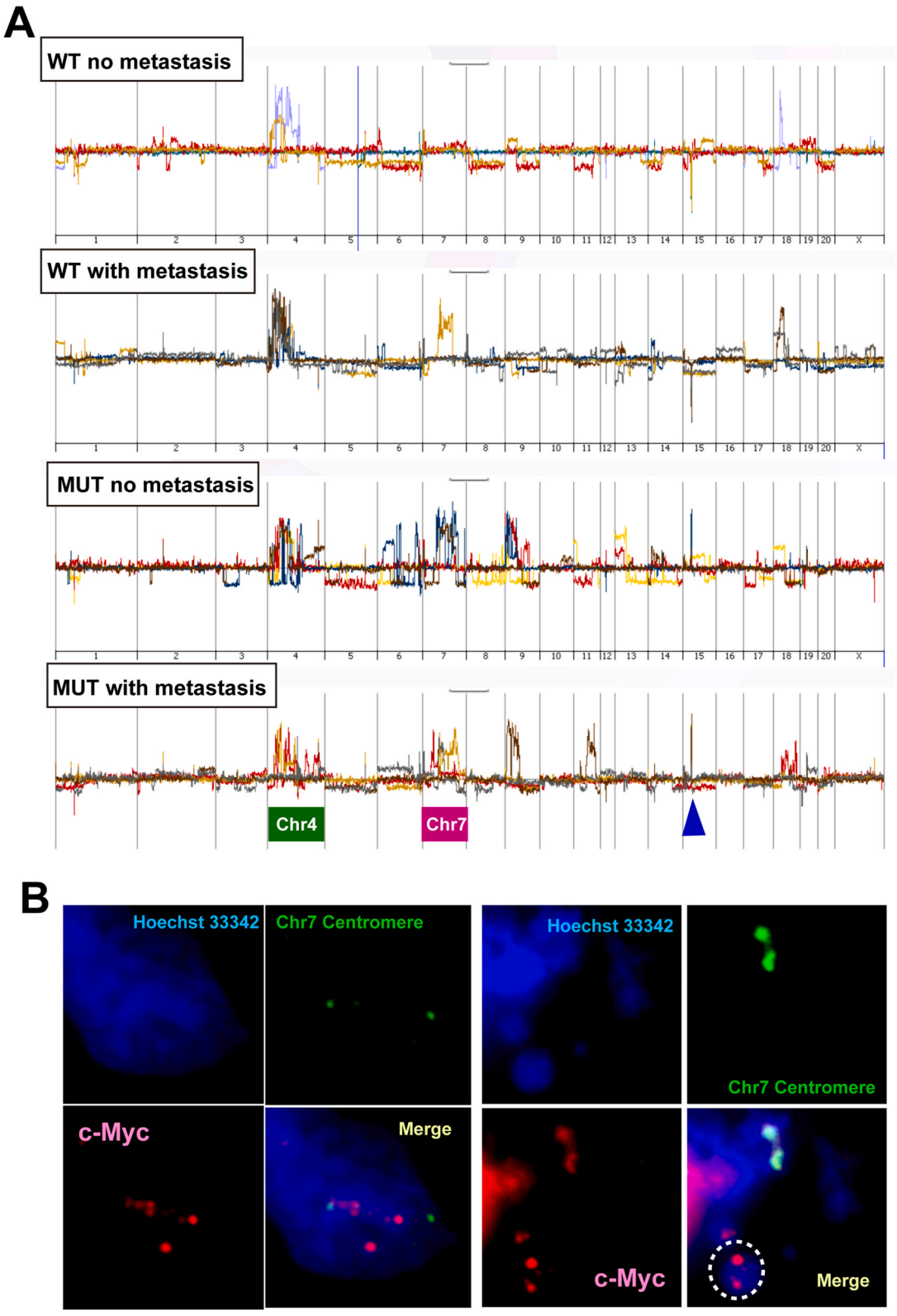


**Fig. 2.** Array-based comparative genome hybridization (aCGH) analysis discloses a preference to chromosomal amplification, including *c-Myc* amplification, in the Fe-NTA-induced RCCs in *Brca1* MUT(L63X/+) rats in comparison to those in the WT rats. (A) Summary of aCGH analysis, which is divided into 4 groups of WT with no pulmonary metastasis (n = 4), WT with pulmonary metastasis (n = 4), MUT with no pulmonary metastasis (n = 4) and MUT with pulmonary metastasis (n = 4). Individual data on all the 16 RCCs are included in Fig. S2 and Table S2. Blue arrowhead, gene-desert area of chromosome 15 with contrasting difference in genomic alteration between WT and MUT RCCs. (B) Representative fluorescent *in situ* hybridization (FISH) analysis of *c-Myc*. *c-Myc* signal/chromosome 7 centromere signal = 7/2 (left 4 panels); extrachromosomal area (micronucleus) includes *c-Myc* amplification (dotted white circle; #C10K3LRCC; right 4 panels). Representative pictures are shown. Refer to text for details.

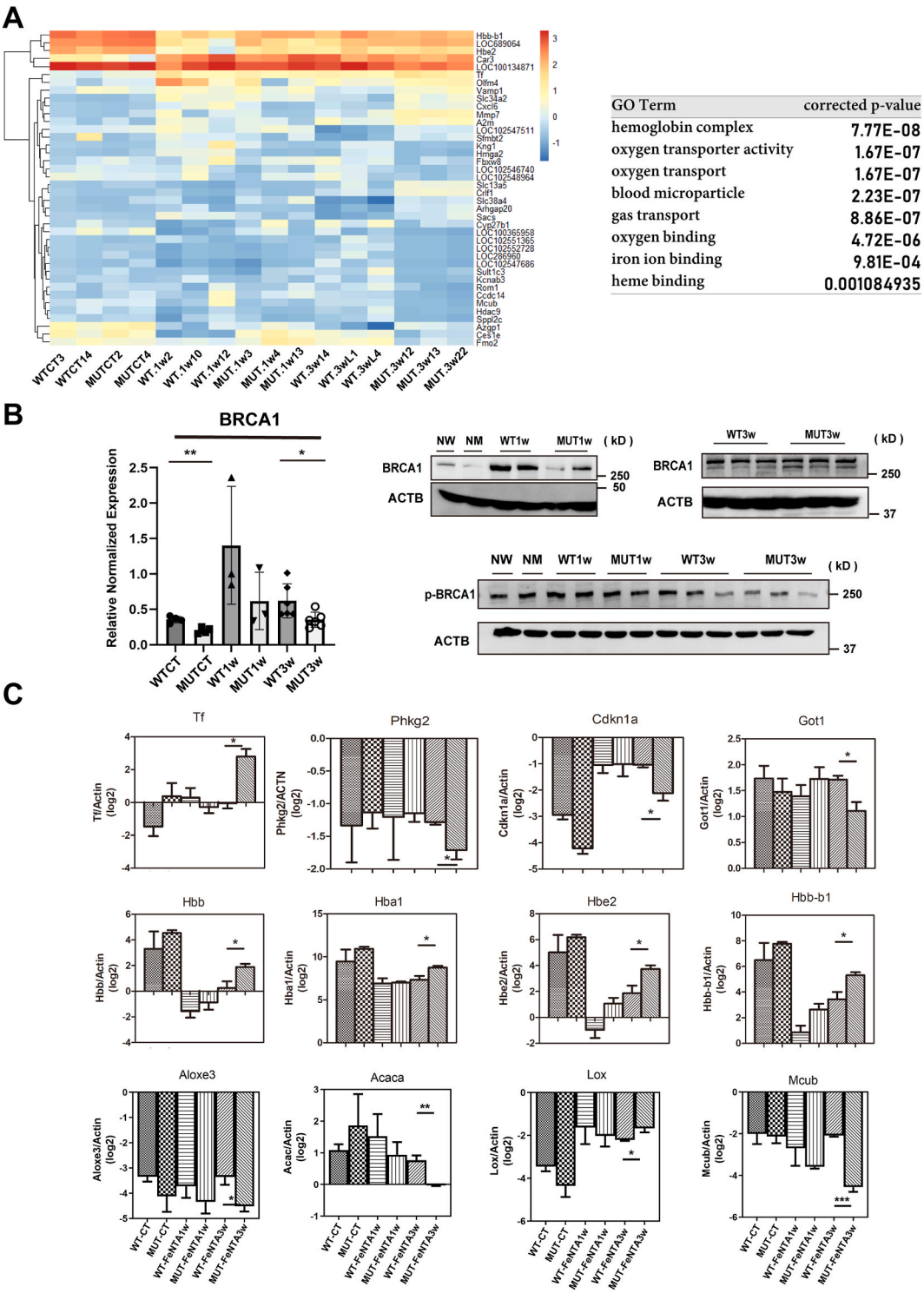


| GO Term | corrected p-value |
|---|---|
| hemoglobin complex | 7.77E-08 |
| oxygen transporter activity | 1.67E-07 |
| oxygen transport | 1.67E-07 |
| blood microparticle | 2.23E-07 |
| gas transport | 8.86E-07 |
| oxygen binding | 4.72E-06 |
| iron ion binding | 9.81E-04 |
| heme binding | 0.001084935 |

**Fig. 3.** Expression microarray analysis at the subacute phase of Fe-NTA-induced renal carcinogenesis sorts out mitochondrial and iron metabolisms as candidate responsible pathways in *Brca1* MUT(L63X/+) rat. (A) Results of hierarchical clustering and GO term analysis for the genes differentially expressed between WT and *Brca1* MUT at 3 weeks in the Fe-NTA-induced renal carcinogenesis protocol (refer to Table S4). (B) Renal *Brca1* expression during the subacute phase of Fe-NTA-induced renal carcinogenesis protocol with qPCR (left panel; means ± SD) and immunoblot analysis (right panels). (C) Examples of altered metabolisms and mitochondrial dysfunction with expression microarray analysis specifically in the kidney of *Brca1* MUT rats during the subacute phase of Fe-NTA-induced renal carcinogenesis (n = 3; $^{*}P < 0.05$, $^{**}P < 0.01$, $^{***}P < 0.001$ *vs wild-type* Fe-NTA renal carcinogenesis protocol at 3 weeks). Refer to text for details.

not only for malignant mesothelioma but also for malignant melanoma and RCC in humans [43] and BAP1 loss defines a new class of RCC [44]. Here we demonstrated that *Brca1* haploinsufficiency significantly promotes Fe-NTA-induced renal carcinogenesis, indicating the usefulness of this rat MUT model to clarify the responsible molecular mechanisms in comparison to various murine models which ended in failure [7]. No significant change between WT and *Brca(L63X/+)* was observed in the final RCC incidence, indicating that promotional effect of *BRCA1* haploinsufficiency is larger than initiation effect in Fe(II)-catalyzed oxidative stress-induced carcinogenesis. CT and MRI scan were helpful to

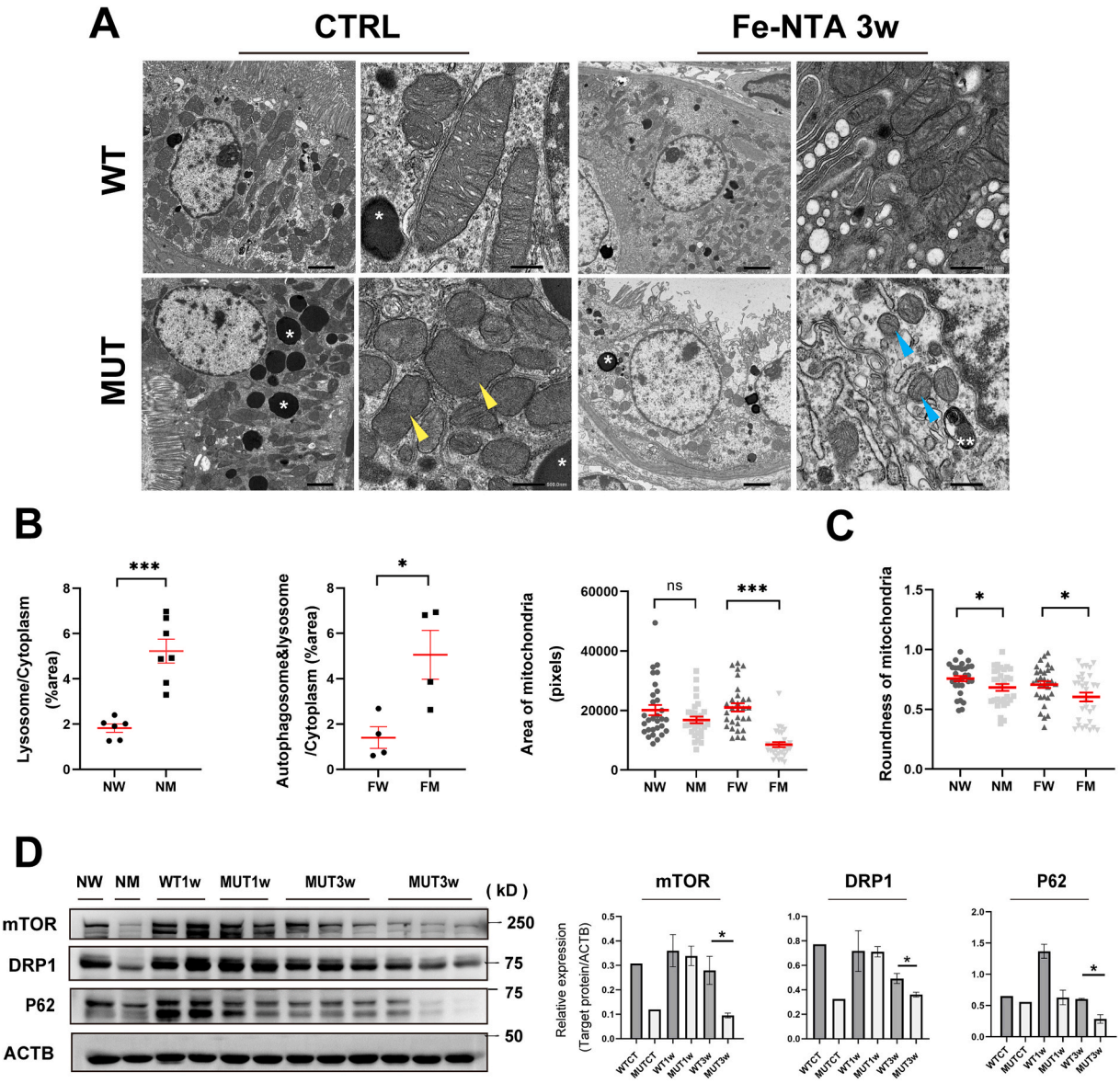


**Fig. 4.** Mitochondrial dysregulation and malfunction in the kidney of in *Brca1* MUT(L63X/+) rat. (A, B) Electron microscopic analysis reveals increased lysosome*/autophagosome** in the renal tubular cells, and small-sized deformed mitochondria with immature cristae formation in the MUT rat in the untreated control (yellow arrowheads) and at 3 weeks in the Fe-NTA-induced renal carcinogenesis protocol (blue arrowheads; bar = 2.0 μm in the left panels; 500 nm in the right panels). (C) Round rate of mitochondria defined as the ratio of the minor axis to the major axis of mitochondria. CTRL, no treatment control; NW, no treatment *wild-type*; NM, no treatment MUT; FW, Fe-NTA-treated *wild-type* at 3 weeks; FM, Fe-NTA-treated MUT at 3 weeks (n = 4–30; ns, not significant, $^{*}P < 0.05$, $^{***}P < 0.001$ *vs wild-type*). (D) Decreased expression of mitochondrial regeneration/fission-associated genes in the kidney of *Brca1* MUT rats during the subacute phase of Fe-NTA-induced renal carcinogenesis (n = 3; $^{*}P < 0.05$ *vs wild-type*). Also refer to Fig. S4 for additional data. (For interpretation of the references to color in this figure legend, the reader is referred to the Web version of this article.)

precisely conclude the diagnosis of RCC prior to autopsy, ruling out other pathologic causes, such as simple renal cyst or ileus.

In our previous study of 2012, using only WT of F1 hybrid rats between *Fischer-344* and *Brown-Norway* strains, chromosomal deletions were prominent in the Fe-NTA-induced RCCs [23], which was confirmed in the present study. We reasoned that smaller amount of genetic information due to deletions would be advantageous for the cancer cells to replicate genomic DNA in the course of persistent proliferation. In contrast, RCCs in the *Brca1(L63X/+)* haploinsufficient rats unexpectedly revealed significantly increased chromosomal amplifications in comparison to those in the WT. Accordingly, we suspect that insufficient amount of Brca1 allows replication of the genome DNA oxidatively damaged but not fully repaired. Currently, gene amplification in extrachromosomal DNA is a hot topic regarding chemotherapy resistance [45]. Extrachromosomal DNA with oncogene amplification is associated with poor outcome across multiple cancers, including breast and renal cancer [46]. This is not only because of the increase in the copy number of oncogene but also of the possibility of rapidly increasing tumor heterogeneity, based on unequal segregation of extrachromosomal DNA from a parental tumor cell to offspring cells [47]. Of note, the current common amplification area (rat chromosome 7) was relatively large and syntenic to chromosomal areas (human chromosome 8) of breast cancers in the Japanese patients with *BRCA1* monoallelic/biallelic loss [26].

We found via target oncogene search on breast cancer that *c-Myc* in rat chromosome 7 is amplified with a significantly higher probability in the RCCs in *Brca1(L63X/+)* haploinsufficient rats. FISH analysis revealed that a major fraction of these are extrachromosomal oncogene amplifications. Therefore, BRCA1 prevents or delays extrachromosomal

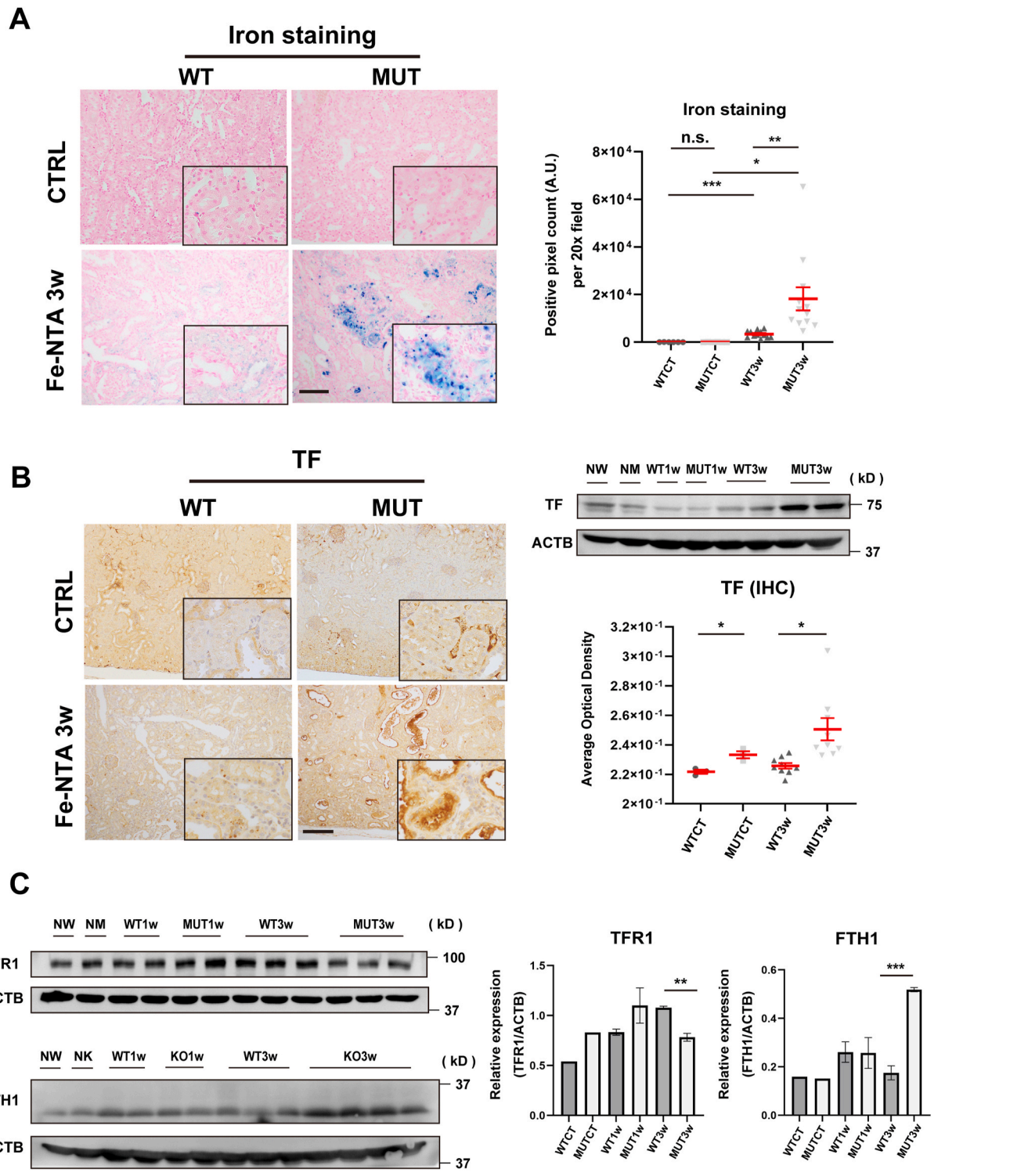


**Fig. 5.** Excess iron accumulation in the kidney of *Brca1* MUT(L63X/+) rat during Fe-NTA-induced renal carcinogenesis. (A) Iron deposition by Perl's iron staining and its quantitation. (B) Immunohistochemical/immunoblot detection of transferrin (Tf). (C) Immunoblot analysis of transferrin receptor 1 (Tfr1) and ferritin heavy chain (Fth1; n = 3; $^{*}P < 0.05$, $^{**}P < 0.01$, $^{***}P < 0.001$ *vs wild-type* Fe-NTA at 3 weeks; bar = 100 μm; 50 μm in the inset in A; 200 μm; 50 μm in the inset in B).

oncogene amplification under oxidative stress. In human breast cancer, *c-Myc* is a driver gene in the present largest functional characterization study [48], *c-Myc* amplification is indeed significantly associated with aggressive tumor phenotype and poor prognosis [49], and *c-Myc* is amplified in *BRCA1*-associated breast cancers [50]. Reportedly, binding of BRCA1 to c-Myc inhibits its transcriptional and transforming activity [51] and BRCA1 and c-Myc associate to transcriptionally repress psoriasin which enhances the sensitivity to etoposide [52]. We believe that whole genome sequencing in the near future with protein functional and signaling studies would clarify more scientific logics why RCCs in the MUT rats show more aggressive behavior with higher proliferation index and peritoneal invasion.

To elucidate the molecular mechanism why Fe-NTA-induced renal carinogenesis is promoted in *Brca1* haploinsufficient rats, we performed

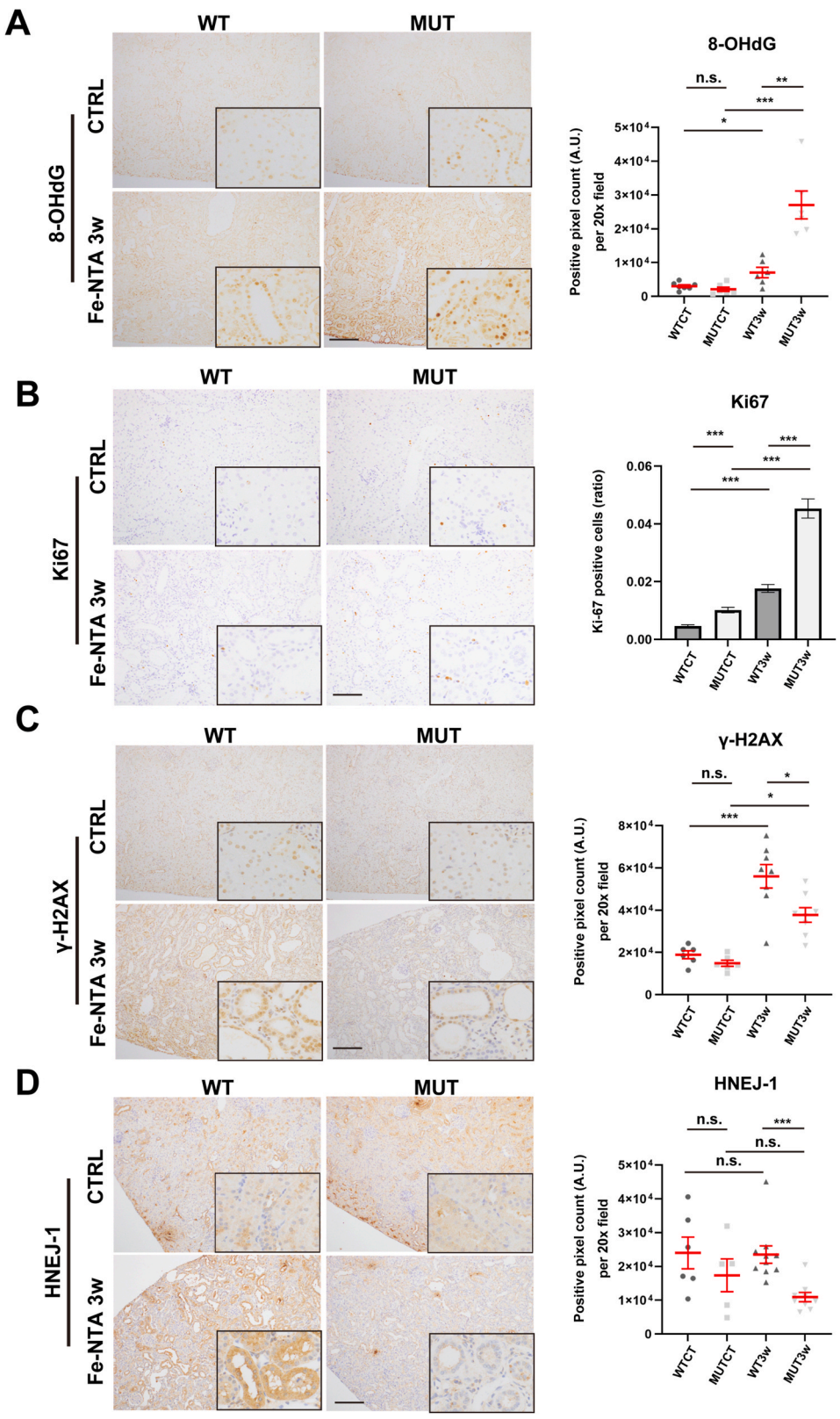


**Fig. 6.** *BRCA1* haploinsufficiency provides both nuclear mutagenic and cytoplasmic ferroptosis-resistant environments. (A) Immunostaining shows higher amounts of 8-OHdG [41] both in the untreated control kidney and in the kidney at 3 weeks of the Fe-NTA-induced renal carcinogenesis protocol of *Brca1* MUT(L63X/+) rat in comparison to WT rat. (B) Ki-67 immunostaining as proliferation index was higher in the *Brca1* MUT kidney than WT at 3 weeks in Fe-NTA-induced renal carcinogenesis protocol. (C) Immunostaining shows higher amounts of γ-H2AX (marker of DNA double-strand breaks [42]) in the kidney at 3 weeks of the Fe-NTA-induced renal carcinogenesis protocol of both WT and *Brca1* MUT rats. However, MUT group reveals significantly lower immunostaining than WT group due to BRCA1 haploinsufficiency, suggesting impaired recognition/repair of DNA double-strand breaks induced by Fe-NTA. Refer to text for details. (D) Immunohistochemistry by HNEJ-1 monoclonal antibody [29] reveals significantly lower positivity in the kidney at 3 weeks of the Fe-NTA-induced renal carcinogenesis protocol in the *Brca1* MUT(L63X/+) rats than WT, indicating that BRCA1 haploinsufficiency more efficiently generates ferroptosis-resistance in response to iron catalyzed oxidative stress (n = 3; $^{*}P < 0.05$, $^{**}P < 0.01$, $^{***}P < 0.001$ *vs wild-type* Fe-NTA at 3 weeks; bar = 200 μm; 50 μm in the inset in A, C and D; 100 μm; 50 μm in the inset in B).

a subacute study on the carcinogenesis protocol for 1 or 3 week(s) to evaluate the early events with histological and expression microarray analyses. We found that iron metabolism is significantly altered in the renal tubules in response to persistent oxidative stress via Fe-NTA. Iron accumulation was significantly higher in the MUT kidney with high iron deposition in the proximal tubular cells not only by iron staining but also by decreased expression of transferrin receptor (Tfr1) and increased expression of ferritin (Fth1) as a feedback. Of note, transferrin (Tf) expression was significantly increased in the MUT kidney after 3-week Fe-NTA administration. Serum transferrin is mainly produced by hepatocytes, but *Tf* expression has been reported in the kidney [53]. Increased urinary Tf excretion characterizes several kinds of acute renal

failure [54]. Tf overexpression was observed at the luminal border of proximal tubular cells and thus appears a strategy of tubular cells to regulate intracellular iron concentration either by releasing or preventing further uptake of iron to escape ferroptosis [10,55]. Precise renal tubular mechanism needs further investigation. However, a recently established ferroptosis marker HNEJ-1 immunostaining [29] as well as Cox-2 and cytoplasmic catalytic Fe(II) was significantly lower in the MUT model after 3-week Fe-NTA administration, indicating ferroptosis-resistance, whereas nuclear 8-OHdG level [31] was significantly higher in the MUT model. These fit well with previous findings that lipophilic antioxidants, such as vitamin E, was preventive in this renal carcinogenesis model [56,57].

To further elucidate the molecular mechanism of the enhanced iron dysregulation in the MUT kidney under persistent Fenton reaction-based oxidative stress, we analyzed expression microarray data, which suggested mitochondrial malfunction by the accumulation of iron- and heme-associated genes. Electron microscopic analysis revealed that mitochondria in the MUT kidney is significantly smaller with deformity, which was significantly aggravated after 3-week Fe-NTA administration with significantly smaller mitochondrial mass. Because mitochondria are a central iron metabolism organelle, including heme and *Fe–S* cluster production [58,59], we assume that mitochondrial dysfunction would dramatically alter the iron distribution intracellularly with *vice versa* [60] and promote the energy acquisition system to be more dependent on glycolytic system as generally established in cancer [61]. Unexpected dissociated maintenance of citrate synthase activity in the MUT kidney after 3-week Fe-NTA administration requires further investigation. We append here that two downregulated cytochrome P450 genes using heme as an active site, *Cyp2d2* and *Cyp27b1*, were included and found decreased in the list of microarray data. *Cyp2d2* is unexpectedly regulated by hnRNP K, a paralogue of PCBP2 playing critical dual roles of transcription regulatory unit and cytosolic Fe(II) chaperone [62,63]. Cyp27b1 activates vitamin $D_3$ to an active form [64,65], which is consistent with the present results in that vitamin $D_3$ is generally cancer preventive [66].

Finally, relative decrease in γ-H2AX, a marker for DNA double-strand breaks [42], in the kidney of Fe-NTA-induced renal carcinogenesis protocol at 3 weeks in MUT in comparison to that of WT may appear contradictory to the previous studies using cultured cells [67–69]. We interpret the decrease in γ-H2AX in *Brca1*-MUT as an impairment of DNA damage recognition and are currently considering various responsible possibilities, including a difference between *in vitro* and *in vivo* situations and abundance of mitochondria, thus iron, in the kidney as discussed above, which needs further investigation. Alternatively, phophorylated Brca1 (S1423) works for cell-cycle G1/S and G2/M checkpoints to regulate the start of replication and mitosis, respectively. Sequential and distinct complexes involving Brca1 have been established with Claspin [70], Herc2 [71], Chk1 [72], *etc.* Sensing DNA damage through ATM (double-strand breaks) [73,74] and ATR (single-strand breaks) [75] initiates this phosphorylation. Therefore, a decrease in phosphorylated Brca1 may eventually cause failure of these checkpoints, leading to genomic amplification.

Here we for the first time demonstrated that *BRCA1* haploinsufficiency causes mitochondrial dysfunction, leading to cellular iron deposition under Fe-NTA-induced renal carcinogenesis model. This can be a carcinogenic driving force to the early establishment of ferroptosis-resistant target cells (Fig. 7). Further, *BRCA1* haploinsufficiency facilitates Fe-NTA-induced renal carcinogenesis at the promotional phase and allows more chromosomal amplifications, including *c-Myc*. *BRCA1* in two normal alleles hence prevents chromosomal amplification under iron-catalyzed persistent oxidative stress, indicating that half an amount of BRCA1 is not sufficient to maintain the genome information unaltered under Fe(II)-catalyzed severe oxidative stress. Therefore, manipulating the iron metabolism, especially at the target organs, can be a preventive strategy of various carcinogenesis for the *BRCA1* germline-mutated patients. Iron reduction as a measure

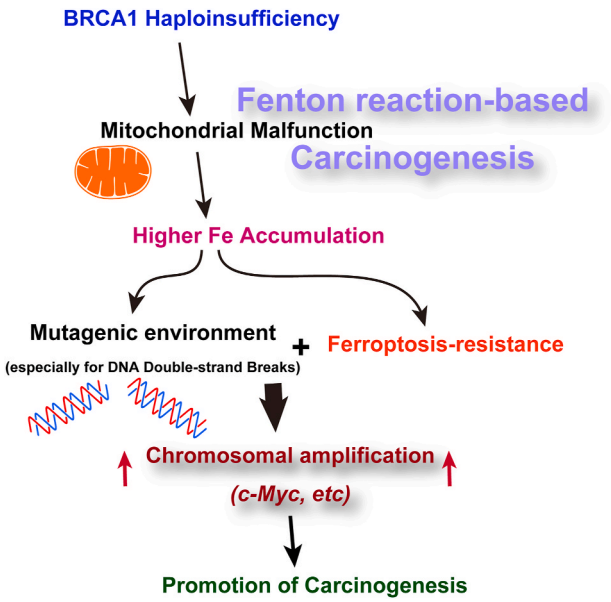


**Fig. 7.** Schematic presentation of the present work.

either by iron chelating agent or phlebotomy was successful for the prevention of malignant mesothelioma at least preclinically [34,76]. Of course, iron deficiency anemia due to menstruation or pregnancy has to be carefully ruled out for considering the procedures. *Brca1(L63X/+)* haploinsufficient rat provides us with a more plausible model than murine models to evaluate possible strategies to increase the quality of life of *BRCA1* germline-mutated patients.

## Author contributions

YK and ST: conception and design of the study; YK, SA, YM, HZ, ZC and YS: acquisition and analysis of the data; YK, SA, YM and ST: drafting the manuscript, the figures and the tables; TM and TI: supply of the *Brca1(L63X/+)* mutant rat.

## Declaration of competing interest

All the authors declare no conflict of interest.

## Acknowledgments

This work was supported, in part, by JST CREST (Grant Number JPMJCR19H4), JSPS Kakenhi (Grant Number JP19H05462 and JP20H05502) and Research Grant of the Princess Takamatsu Cancer Research Fund (19–25126) to ST; JSPS Kakenhi (Grant Number JP16H06276[AdAMS]) to TM and JP21H03601 to TI. This work was financially supported by JST SPRING, Grant Number JPMJSP2125 to YK. The author (YK) would like to take this opportunity to thank the "Interdisciplinary Frontier Next-Generation Researcher Program of the 10 Tokai Higher Education and Research System." The authors thank Nobuaki Misawa (Department of Pathology and Biological Responses, Nagoya University Graduate School of Medicine) for excellent technical assistance. Electron microscopic analyses were supported by Koji Itakura, Division of Medical Research Engineering, Nagoya University Graduate School of Medicine.

## Appendix A. Supplementary data

Supplementary data to this article can be found online at https://doi.org/10.1016/j.redox.2022.102356.

## References


[1] B. Vogelstein, K.W. Kinzler, The Genetic Basis of Human Cancer, McGraw-Hill, New York, 1998.

[2] Y. Miki, J. Swensen, D. Shattuck-Eidens, P.A. Futreal, K. Harshman, S. Tavtigian, Q. Liu, C. Cochran, L.M. Bennett, W. Ding, et al., A strong candidate for the breast and ovarian cancer susceptibility gene BRCA1, Science 266 (5182) (1994) 66–71.

[3] A. Liede, B.Y. Karlan, S.A. Narod, Cancer risks for male carriers of germline mutations in BRCA1 or BRCA2: a review of the literature, J. Clin. Oncol. 22 (4) (2004) 735–742.

[4] H. Cavanagh, K.M. Rogers, The role of BRCA1 and BRCA2 mutations in prostate, pancreatic and stomach cancers, Hered. Cancer Clin. Pract. 13 (1) (2015) 16.

[5] S.A. Narod, W.D. Foulkes, BRCA1 and BRCA2: 1994 and beyond, Nat. Rev. Cancer 4 (9) (2004) 665–676.

[6] N.M. Tung, J.C. Boughey, L.J. Pierce, M.E. Robson, I. Bedrosian, J.R. Dietz, A. Dragun, J.B. Gelpi, E.W. Hofstatter, C.J. Isaacs, I. Jatoi, E. Kennedy, J.K. Litton, N.A. Mayr, R.D. Qamar, M.G. Trombetta, B.E. Harvey, M.R. Somerfield, D. Zakalik, Management of hereditary breast cancer: American society of clinical oncology, American society for radiation oncology, and society of surgical oncology guideline, J. Clin. Oncol. 38 (18) (2020) 2080–2106.

[7] B. Evers, J. Jonkers, Mouse models of BRCA1 and BRCA2 deficiency: past lessons, current understanding and future prospects, Oncogene 25 (43) (2006) 5885–5897.

[8] S. Akatsuka, G.H. Li, S. Toyokuni, Superiority of rat over murine model for studies on the evolution of cancer genome, Free Radic. Res. 52 (11–12) (2018) 1323–1327.

[9] S. Toyokuni, Role of iron in carcinogenesis: cancer as a ferrotoxic disease, Cancer Sci. 100 (1) (2009) 9–16.

[10] S. Toyokuni, F. Ito, K. Yamashita, Y. Okazaki, S. Akatsuka, Iron and thiol redox signaling in cancer: an exquisite balance to escape ferroptosis, Free Radic. Biol. Med. 108 (2017) 610–626.

[11] S.V. Torti, D.H. Manz, B.T. Paul, N. Blanchette-Farra, F.M. Torti, Iron and cancer, Annu. Rev. Nutr. 38 (2018) 97–125.

[12] S. Toyokuni, I. Yanatori, Y. Kong, H. Zheng, Y. Motooka, L. Jiang, Ferroptosis at the crossroads of infection, aging and cancer, Cancer Sci. 111 (2020) 2665–2671.

[13] S. Toyokuni, Y. Kong, Z. Cheng, K. Sato, S. Hayashi, F. Ito, L. Jiang, I. Yanatori, Y. Okazaki, S. Akatsuka, Carcinogenesis as side effects of iron and oxygen utilization: from the unveiled truth toward ultimate bioengineering, Cancers 12 (11) (2020) 3320.

[14] J. Kotsopoulos, G. Sukiennicki, M. Muszynska, D. Gackowski, K. Kaklewski, K. Durda, K. Jaworska, T. Huzarski, J. Gronwald, T. Byrski, O. Ashuryk, T. Debniak, A. Toloczko-Grabarek, M. Stawicka, D. Godlewski, R. Olinski, A. Jakubowska, S. A. Narod, J. Lubinski, Plasma micronutrients, trace elements, and breast cancer in BRCA1 mutation carriers: an exploratory study, Cancer Causes Control 23 (7) (2012) 1065–1074.

[15] S. Toyokuni, K. Uchida, K. Okamoto, Y. Hattori-Nakakuki, H. Hiai, E.R. Stadtman, Formation of 4-hydroxy-2-nonenal-modified proteins in the renal proximal tubules of rats treated with a renal carcinogen, ferric nitrilotriacetate, Proc. Natl. Acad. Sci. U.S.A. 91 (1994) 2616–2620.

[16] S. Toyokuni, T. Mori, M. Dizdaroglu, DNA base modifications in renal chromatin of Wistar rats treated with a renal carcinogen, ferric nitrilotriacetate, Int. J. Cancer 57 (1994) 123–128.

[17] S. Toyokuni, T. Mori, H. Hiai, M. Dizdaroglu, Treatment of Wistar rats with a renal carcinogen, ferric nitrilotriacetate, causes DNA-protein cross-linking between thymine and tyrosine in their renal chromatin, Int. J. Cancer 62 (1995) 309–313.

[18] S. Toyokuni, X.P. Luo, T. Tanaka, K. Uchida, H. Hiai, D.C. Lehotay, Induction of a wide range of $C_{2\text{-}12}$ aldehydes and $C_{7\text{-}12}$ acyloins in the kidney of Wistar rats after treatment with a renal carcinogen, ferric nitrilotriacetate, Free Radic. Biol. Med. 22 (1997) 1019–1027.

[19] Y. Ebina, S. Okada, S. Hamazaki, F. Ogino, J.L. Li, O. Midorikawa, Nephrotoxicity and renal cell carcinoma after use of iron- and aluminum- nitrilotriacetate complexes in rats, J. Natl. Cancer Inst. 76 (1986) 107–113.

[20] Y. Nishiyama, H. Suwa, K. Okamoto, M. Fukumoto, H. Hiai, S. Toyokuni, Low incidence of point mutations in H-, K- and N-ras oncogenes and p53 tumor suppressor gene in renal cell carcinoma and peritoneal mesothelioma of Wistar rats induced by ferric nitrilotriacetate, Jpn. J. Cancer Res. 86 (1995) 1150–1158.

[21] T. Tanaka, Y. Iwasa, S. Kondo, H. Hiai, S. Toyokuni, High incidence of allelic loss on chromosome 5 and inactivation of p15 $^{INK4B}$ and p16 $^{INK4A}$ tumor suppressor genes in oxystress-induced renal cell carcinoma of rats, Oncogene 18 (1999) 3793–3797.

[22] M. Hiroyasu, M. Ozeki, H. Kohda, M. Echizenya, T. Tanaka, H. Hiai, S. Toyokuni, Specific allelic loss of p16 (INK4A) tumor suppressor gene after weeks of iron-mediated oxidative damage during rat renal carcinogenesis, Am. J. Pathol. 160 (2) (2002) 419–424.

[23] S. Akatsuka, Y. Yamashita, H. Ohara, Y.T. Liu, M. Izumiya, K. Abe, M. Ochiai, L. Jiang, H. Nagai, Y. Okazaki, H. Murakami, Y. Sekido, E. Arai, Y. Kanai, O. Hino, T. Takahashi, H. Nakagama, S. Toyokuni, Fenton reaction induced cancer in wild type rats recapitulates genomic alterations observed in human cancer, PLoS One 7 (8) (2012), e43403.

[24] S. Toyokuni, The origin and future of oxidative stress pathology: from the recognition of carcinogenesis as an iron addiction with ferroptosisresistance to non-thermal plasma therapy, Pathol. Int. 66 (2016) 245–259.

[25] O.A. Stefansson, J.G. Jonasson, O.T. Johannsson, K. Olafsdottir, M. Steinarsdottir, S. Valgeirsdottir, J.E. Eyfjord, Genomic profiling of breast tumours in relation to BRCA abnormalities and phenotypes, Breast Cancer Res. 11 (4) (2009) R47.

[26] Y. Inagaki-Kawata, K. Yoshida, N. Kawaguchi-Sakita, M. Kawashima, T. Nishimura, N. Senda, Y. Shiozawa, Y. Takeuchi, Y. Inoue, A. Sato-Otsubo, Y. Fujii, Y. Nannya, E. Suzuki, M. Takada, H. Tanaka, Y. Shiraishi, K. Chiba, Y. Kataoka, M. Torii, H. Yoshibayashi, K. Yamagami, R. Okamura, Y. Moriguchi, H. Kato, S. Tsuyuki, A. Yamauchi, H. Suwa, T. Inamoto, S. Miyano, S. Ogawa, M. Toi, Genetic and clinical landscape of breast cancers with germline BRCA1/2 variants, Commun Biol 3 (1) (2020) 578.

[27] S. Toyokuni, S. Okada, S. Hamazaki, M. Fujioka, J.-L. Li, O. Midorikawa, Cirrhosis of the liver induced by cupric nitrilotriacetate in Wistar rats: an experimetnal model of copper toxicosis, Am. J. Pathol. 134 (1989) 1263–1274.

[28] L. Jiang, H. Zheng, Q. Lyu, S. Hayashi, K. Sato, Y. Sekido, K. Nakamura, H. Tanaka, K. Ishikawa, H. Kajiyama, M. Mizuno, M. Hori, S. Toyokuni, Lysosomal nitric oxide determines transition from autophagy to ferroptosis after exposure to plasma-activated Ringer's lactate, Redox Biol. 43 (2021) 101989.

[29] H. Zheng, L. Jiang, T. Tsuduki, M. Conrad, S. Toyokuni, Embryonal erythropoiesis and aging exploit ferroptosis, Redox Biol. 48 (2021) 102175.

[30] Z. Cheng, S. Akatsuka, G.H. Li, K. Mori, T. Takahashi, S. Toyokuni, Ferroptosis-resistance determines high susceptibility of murine A/J strain to iron-induced renal carcinogenesis, Cancer Sci. 113 (2021) 65–78.

[31] S. Toyokuni, Reactive oxygen species-induced molecular damage and its application in pathology, Pathol. Int. 49 (1999) 91–102.

[32] K. Yamashita, K. Kohashi, Y. Yamada, T. Ishii, Y. Nishida, H. Urakawa, I. Ito, M. Takahashi, T. Inoue, M. Ito, Y. Ohara, Y. Oda, S. Toyokuni, Osteogenic differentiation in dedifferentiated liposarcoma: a study of 36 cases in comparison to the cases without ossification, Histopathology 72 (5) (2018) 729–738.

[33] F. Ito, T. Nishiyama, L. Shi, M. Mori, T. Hirayama, H. Nagasawa, H. Yasui, S. Toyokuni, Contrasting intra- and extracellular distribution of catalytic ferrous iron in ovalbumin-induced peritonitis, Biochem. Biophys. Res. Commun. 476 (4) (2016) 600–606.

[34] H. Nagai, Y. Okazaki, S.H. Chew, N. Misawa, H. Yasui, S. Toyokuni, Deferasirox induces mesenchymal-epithelial transition in crocidolite-induced mesothelial carcinogenesis in rats, Cancer Prev. Res. 6 (2013) 1222–1230.

[35] L. Yue, Y. Luo, L. Jiang, Y. Sekido, S. Toyokuni, PCBP2 knockdown promotes ferroptosis in malignant mesothelioma, Pathol. Int. 72 (4) (2022) 242–251.

[36] R.A. Weinberg, The Biology of Cancer, 2 ed., Garland Science, Tailor & Francis Group, LLC, New York, 2014.

[37] G. Novara, G. Martignoni, W. Artibani, V. Ficarra, Grading systems in renal cell carcinoma, J. Urol. 177 (2) (2007) 430–436.

[38] M. Adebayo, S. Singh, A.P. Singh, S. Dasgupta, Mitochondrial fusion and fission: the fine-tune balance for cellular homeostasis, Faseb. J. 35 (6) (2021), e21620.

[39] M. Morita, S.P. Gravel, L. Hulea, O. Larsson, M. Pollak, J. St-Pierre, I. Topisirovic, mTOR coordinates protein synthesis, mitochondrial activity and proliferation, Cell Cycle 14 (4) (2015) 473–480.

[40] D.P. Panigrahi, P.P. Praharaj, C.S. Bhol, K.K. Mahapatra, S. Patra, B.P. Behera, S. R. Mishra, S.K. Bhutia, The emerging, multifaceted role of mitophagy in cancer and cancer therapeutics, Semin. Cancer Biol. 66 (2020) 45–58.

[41] S. Toyokuni, T. Tanaka, Y. Hattori, Y. Nishiyama, H. Ochi, H. Hiai, K. Uchida, T. Osawa, Quantitative immunohistochemical determination of 8-hydroxy-2'-deoxyguanosine by a monoclonal antibody N45.1: its application to ferric nitrilotriacetate-induced renal carcinogenesis model, Lab. Invest. 76 (1997) 365–374.

[42] L.J. Kuo, L.X. Yang, Gamma-H2AX - a novel biomarker for DNA double-strand breaks, in: Vivo, vol. 22, 2008, pp. 305–309, 3.

[43] J.R. Testa, M. Cheung, J. Pei, J.E. Below, Y. Tan, E. Sementino, N.J. Cox, A. U. Dogan, H.I. Pass, S. Trusa, M. Hesdorffer, M. Nasu, A. Powers, Z. Rivera, S. Comertpay, M. Tanji, G. Gaudino, H. Yang, M. Carbone, Germline BAP1 mutations predispose to malignant mesothelioma, Nat. Genet. 43 (10) (2011) 1022–1025.

[44] S. Peña-Llopis, S. Vega-Rubín-de-Celis, A. Liao, N. Leng, A. Pavía-Jiménez, S. Wang, T. Yamasaki, L. Zhrebker, S. Sivanand, P. Spence, BAP1 loss defines a new class of renal cell carcinoma, Nat. Genet. 44 (7) (2012) 751.

[45] D.G. Albertson, Gene amplification in cancer, Trends Genet. 22 (8) (2006) 447–455.

[46] H. Kim, N.P. Nguyen, K. Turner, S. Wu, A.D. Gujar, J. Luebeck, J. Liu, V. Deshpande, U. Rajkumar, S. Namburi, S.B. Amin, E. Yi, F. Menghi, J.H. Schulte, A.G. Henssen, H.Y. Chang, C.R. Beck, P.S. Mischel, V. Bafna, R.G.W. Verhaak, Extrachromosomal DNA is associated with oncogene amplification and poor outcome across multiple cancers, Nat. Genet. 52 (9) (2020) 891–897.

[47] R.G.W. Verhaak, V. Bafna, P.S. Mischel, Extrachromosomal oncogene amplification in tumour pathogenesis and evolution, Nat. Rev. Cancer 19 (5) (2019) 283–288.

[48] R. Marcotte, A. Sayad, K.R. Brown, F. Sanchez-Garcia, J. Reimand, M. Haider, C. Virtanen, J.E. Bradner, G.D. Bader, G.B. Mills, D. Pe'er, J. Moffat, B.G. Neel, Functional genomic landscape of human breast cancer drivers, vulnerabilities, and resistance, Cell 164 (1–2) (2016) 293–309.

[49] Y. Chen, O.I. Olopade, MYC in breast tumor progression, Expert Rev. Anticancer Ther. 8 (10) (2008) 1689–1698.

[50] T.A. Grushko, J.J. Dignam, S. Das, A.M. Blackwood, C.M. Perou, K.K. Ridderstrale, K.N. Anderson, M.J. Wei, A.J. Adams, F.G. Hagos, L. Sveen, H.T. Lynch, B. L. Weber, O.I. Olopade, MYC is amplified in BRCA1-associated breast cancers, Clin. Cancer Res. 10 (2) (2004) 499–507.

[51] Q. Wang, H. Zhang, K. Kajino, M.I. Greene, BRCA1 binds c-Myc and inhibits its transcriptional and transforming activity in cells, Oncogene 17 (15) (1998) 1939–1948.

[52] R.D. Kennedy, J.J. Gorski, J.E. Quinn, G.E. Stewart, C.R. James, S. Moore, K. Mulligan, E.D. Emberley, T.F. Lioe, P.J. Morrison, P.B. Mullan, G. Reid, P. G. Johnston, P.H. Watson, D.P. Harkin, BRCA1 and c-Myc associate to transcriptionally repress psoriasin, a DNA damage-inducible gene, Cancer Res. 65 (22) (2005) 10265–10272.

[53] R.L. Idzerda, H. Huebers, C.A. Finch, G.S. McKnight, Rat transferrin gene expression: tissue-specific regulation by iron deficiency, Proc. Natl. Acad. Sci. U.S.A. 83 (11) (1986) 3723–3727.
[54] A.G. Casanova, L. Vicente-Vicente, M.T. Hernandez-Sanchez, M. Prieto, M. I. Rihuete, L.M. Ramis, E. Del Barco, J.J. Cruz, A. Ortiz, I. Cruz-Gonzalez, C. Martinez-Salgado, M. Pescador, F.J. Lopez-Hernandez, A.I. Morales, Urinary transferrin pre-emptively identifies the risk of renal damage posed by subclinical tubular alterations, Biomed. Pharmacother. 121 (2020) 109684.
[55] B.R. Stockwell, J.P. Friedmann Angeli, H. Bayir, A.I. Bush, M. Conrad, S.J. Dixon, S. Fulda, S. Gascon, S.K. Hatzios, V.E. Kagan, K. Noel, X. Jiang, A. Linkermann, M. E. Murphy, M. Overholtzer, A. Oyagi, G.C. Pagnussat, J. Park, Q. Ran, C. S. Rosenfeld, K. Salnikow, D. Tang, F.M. Torti, S.V. Torti, S. Toyokuni, K. A. Woerpel, D.D. Zhang, Ferroptosis: a regulated cell death nexus linking metabolism, Redox Biol. Dise. Cell. 171 (2) (2017) 273–285.
[56] S. Okada, S. Hamazaki, Y. Ebina, J.-L. Li, O. Midorikawa, Nephrotoxicity and its prevention by vitamin E on ferric nitrilotriacetate-promoted lipid peroxidation, Biochim. Biophys. Acta 922 (1987) 28–33.
[57] S. Hamazaki, S. Okada, Y. Ebina, J.L. Li, O. Midorikawa, Effect of dietary vitamin E on ferric nitrilotriacetate-induced nephrotoxicity in rats, Toxicol. Appl. Pharmacol. 92 (1988) 500–506.
[58] M. Whitnall, Y. Suryo Rahmanto, M.L. Huang, F. Saletta, H.C. Lok, L. Gutierrez, F. J. Lazaro, A.J. Fleming, T.G. St Pierre, M.R. Mikhael, P. Ponka, D.R. Richardson, Identification of nonferritin mitochondrial iron deposits in a mouse model of Friedreich ataxia, Proc. Natl. Acad. Sci. U.S.A. 109 (50) (2012) 20590–20595.
[59] J.J. Braymer, R. Lill, Iron-sulfur cluster biogenesis and trafficking in mitochondria, J. Biol. Chem. 292 (31) (2017) 12754–12763.
[60] B.T. Paul, D.H. Manz, F.M. Torti, S.V. Torti, Mitochondria and Iron: current questions, Expet Rev. Hematol. 10 (1) (2017) 65–79.
[61] D. Hanahan, R.A. Weinberg, Hallmarks of cancer: the next generation, Cell 144 (5) (2011) 646–674.
[62] I. Yanatori, D.R. Richardson, S. Toyokuni, F. Kishi, The iron chaperone poly(rC)-binding protein 2 forms a metabolon with the heme oxygenase 1/cytochrome P450 reductase complex for heme catabolism and iron transfer, J. Biol. Chem. 292 (32) (2017) 13205–13229.
[63] I. Yanatori, D.R. Richardson, S. Toyokuni, F. Kishi, The new role of poly (rC)-binding proteins as iron transport chaperones: proteins that could couple with inter-organelle interactions to safely traffic iron, Biochim. Biophys. Acta Gen. Subj. 1864 (11) (2020) 129685.
[64] D.R. Fraser, E. Kodicek, Unique biosynthesis by kidney of a biological active vitamin D metabolite, Nature 228 (5273) (1970) 764–766.
[65] J.G. Ghazarian, C.R. Jefcoate, J.C. Knutson, W.H. Orme-Johnson, H.F. DeLuca, Mitochondrial cytochrome p450. A component of chick kidney 25-hydrocholecalciferol-1alpha-hydroxylase, J. Biol. Chem. 249 (10) (1974) 3026–3033.
[66] W.B. Grant, A review of the evidence supporting the vitamin D-cancer prevention hypothesis in 2017, Anticancer Res. 38 (2) (2018) 1121–1136.
[67] S.A. Krum, E. la Rosa Dalugdugan, G.A. Miranda-Carboni, T.F. Lane, BRCA1 forms a functional complex with gamma-H2AX as a late response to genotoxic stress, J. Nucleic Acids 2010 (2010) 801594.
[68] K.I. Savage, K.B. Matchett, E.M. Barros, K.M. Cooper, G.W. Irwin, J.J. Gorski, K. S. Orr, J. Vohhodina, J.N. Kavanagh, A.F. Madden, A. Powell, L. Manti, S. S. McDade, B.H. Park, K.M. Prise, S.A. McIntosh, M. Salto-Tellez, D.J. Richard, C. T. Elliott, D.P. Harkin, BRCA1 deficiency exacerbates estrogen-induced DNA damage and genomic instability, Cancer Res. 74 (10) (2014) 2773–2784.
[69] R.C. West, G.J. Bouma, Q.A. Winger, Shifting perspectives from "oncogenic" to oncofetal proteins; how these factors drive placental development, Reprod. Biol. Endocrinol. 16 (1) (2018) 101.
[70] S.Y. Lin, K. Li, G.S. Stewart, S.J. Elledge, Human Claspin works with BRCA1 to both positively and negatively regulate cell proliferation, Proc. Natl. Acad. Sci. U.S.A. 101 (17) (2004) 6484–6489.
[71] N. Izawa, W. Wu, K. Sato, H. Nishikawa, A. Kato, N. Boku, F. Itoh, T. Ohta, HERC2 Interacts with Claspin and regulates DNA origin firing and replication fork progression, Cancer Res. 71 (17) (2011) 5621–5625.
[72] R.I. Yarden, S. Pardo-Reoyo, M. Sgagias, K.H. Cowan, L.C. Brody, BRCA1 regulates the G2/M checkpoint by activating Chk1 kinase upon DNA damage, Nat. Genet. 30 (3) (2002) 285–289.
[73] D. Cortez, Y. Wang, J. Qin, S.J. Elledge, Requirement of ATM-dependent phosphorylation of brca1 in the DNA damage response to double-strand breaks, Science 286 (5442) (1999) 1162–1166.
[74] N. Foray, D. Marot, A. Gabriel, V. Randrianarison, A.M. Carr, M. Perricaudet, A. Ashworth, P. Jeggo, A subset of ATM- and ATR-dependent phosphorylation events requires the BRCA1 protein, EMBO J. 22 (11) (2003) 2860–2871.
[75] R.S. Tibbetts, D. Cortez, K.M. Brumbaugh, R. Scully, D. Livingston, S.J. Elledge, R. T. Abraham, Functional interactions between BRCA1 and the checkpoint kinase ATR during genotoxic stress, Genes Dev. 14 (23) (2000) 2989–3002.
[76] Y. Ohara, S.H. Chew, T. Shibata, Y. Okazaki, K. Yamashita, S. Toyokuni, Phlebotomy as a preventive measure for crocidolite-induced mesothelioma in male rats, Cancer Sci. 109 (2) (2018) 330–339.